

Review

Advanced Magnetic Resonance Imaging Modalities for Breast Cancer Diagnosis: An Overview of Recent Findings and Perspectives

Daryoush Shahbazi-Gahrouei ^{1,*}, Fahimeh Aminolroayaei ¹, Hamide Nematollahi ¹, Mohammad Ghaderian ¹ and Sogand Shahbazi Gahrouei ²

¹ Department of Medical Physics, School of Medicine, Isfahan University of Medical Sciences, Isfahan 8174673461, Iran

² Department of Management, School of Humanities, Najafabad Branch, Islamic Azad University, Najafabad 8514143131, Iran

* Correspondence: shahbazi@med.mui.ac.ir; Tel.: +98-31-37929095; Fax: +98-31-36688597

Abstract: Breast cancer is the most prevalent cancer among women and the leading cause of death. Diffusion-weighted imaging (DWI) and diffusion tensor imaging (DTI) are advanced magnetic resonance imaging (MRI) procedures that are widely used in the diagnostic and treatment evaluation of breast cancer. This review article describes the characteristics of new MRI methods and reviews recent findings on breast cancer diagnosis. This review study was performed on the literature sourced from scientific citation websites such as Google Scholar, PubMed, and Web of Science until July 2021. All relevant works published on the mentioned scientific citation websites were investigated. Because of the propensity of malignancies to limit diffusion, DWI can improve MRI diagnostic specificity. Diffusion tensor imaging gives additional information about diffusion directionality and anisotropy over traditional DWI. Recent findings showed that DWI and DTI and their characteristics may facilitate earlier and more accurate diagnosis, followed by better treatment. Overall, with the development of instruments and novel MRI modalities, it may be possible to diagnose breast cancer more effectively in the early stages.

Keywords: diagnosis; MRI; diffusion tensor imaging; diffusion-weighted imaging; breast cancer



Citation: Shahbazi-Gahrouei, D.; Aminolroayaei, F.; Nematollahi, H.; Ghaderian, M.; Gahrouei, S.S. Advanced Magnetic Resonance Imaging Modalities for Breast Cancer Diagnosis: An Overview of Recent Findings and Perspectives. *Diagnostics* **2022**, *12*, 2741. <https://doi.org/10.3390/diagnostics12112741>

Academic Editor: Ernesto Di Cesare

Received: 8 October 2022

Accepted: 7 November 2022

Published: 9 November 2022

Publisher's Note: MDPI stays neutral with regard to jurisdictional claims in published maps and institutional affiliations.



Copyright: © 2022 by the authors. Licensee MDPI, Basel, Switzerland. This article is an open access article distributed under the terms and conditions of the Creative Commons Attribution (CC BY) license (<https://creativecommons.org/licenses/by/4.0/>).

1. Introduction

Breast cancer is the most prevalent cancer in women [1]. Magnetic resonance imaging (MRI) has been drastically utilized to detect breast cancer due to its high contrast resolution. In the past few decades, developments in instruments, contrast agents, and modalities have brought MRI into a new era of breast cancer diagnosis [1,2]. MR imaging modalities include T₂-weighted imaging, dynamic contrast-enhanced imaging (DCE-MRI), diffusion-weighted imaging (DWI), diffusion tensor imaging (DTI), and MR spectroscopy (MRS). Although routine MRI has a high sensitivity (80–100%) among these techniques, it lacks characterization specificity for breast cancer [3]. Even though there is still a substantial link between DCE-MRI and tumor vascular structures, there is no confirmation that this approach is connected with tumor cellular proliferation [4]. Moreover, DCE-MRI specificity can be as low as 37% or as high as 97%. However, the development of DCE-MRI involves higher costs than other techniques, and it cannot be utilized with contrast agents for patients with renal dysfunction [5]. Therefore, multimodality imaging may cover some limitations of MRI models [6]. Diffusion-weighted imaging is helpful to measure the portability of water particles diffusing in tissue. Its technological benefits include a fast acquisition period (usually three min), vast accessibility to various commercial scanners, and no requirement for administering contrast agents [7]. On the other hand, its limitation is sensitivity to artifacts such as T₂ shine through, T₂ blackout, ghosting, blurring, and distortions [8].

Generally, diffusion is measured qualitatively on trace images and quantitatively by the apparent diffusion coefficient (ADC), a parameter that can be used to map the limited diffusion of tissues on the trace image and hypointense [8]. During post-processing, ADC is calculated using at least two distinct b values. The literature indicates that the ADC value is the slope of a line superimposed on the relative signal intensity (y-axis) logarithm plot versus the b value (x-axis). An ADC map refers to the ultimate image with different ADC values determined for each image pixel. It is noted that ADC maps contain weak anatomical details and can be studied alongside other MRI images [9]. Most breast tumors (75–80%) are positive for estrogen receptors, and ~75% of them are positive for progesterone receptors [10]. Variations in ADC values according to estrogen or progesterone receptor expression have been documented in different studies [11–13]. Tumors that are positive for estrogen or progesterone receptors appear to have fewer ADC values than those which are negative [14]. The capacity of ADC measurements to distinguish between benign and malignant non-mass-like enhancement lesions is limited. Therefore, for non-mass-like enhancement lesions relative to mass lesions, a higher ADC value cutoff might be appropriate [15]. DWI is usually carried out before the administration of contrast. Additionally, it can be conducted following a contrast decrease in the ADC value [3]. According to studies, when diffusion is performed after DCE-MRI, a contrast agent may reduce the ADC value. However, after contrast administration with fat suppression (STIR technique), no critical effect has been demonstrated [16,17]. A DCE-MRI protocol exclusive to one non-contrast phase and one post-contrast phase has also received consideration to evaluate breast cancer [18,19]. Numerous research studies have shown that the detection rate of a DWI-based abbreviated unenhanced MRI protocol is comparable to a contrast-enhanced (CE) abbreviated protocol [20–22].

Water diffuses freely and isotropically in most conditions. When impenetrable barriers are encountered, it becomes anisotropic with an ellipsoidal shape [23], with rapid, unrestricted diffusion by the boundaries and slower, constrained diffusion vertical to the boundaries, based on the cell size and density. Diffusion in the ductal/glandular system is rapid due to the breast's high water content and low cell density. When cancer cells obstruct the ducts and lobules, water transport is restricted, decreasing diffusion coefficients in all directions [24]. Although DWI does not detect this ellipsoidal shape, DTI has overcome this restriction. Theoretically, in DTI, at least six independent diffusion gradients measurements accompanied by six non-collinear directions are needed to evaluate all diffusion tensor elements [23]. At present, the most commonly used invariant anisotropy test is fractional anisotropy (FA) [25]. However, the FA has defined no complete tensor form or distribution because different combinations of eigenvalues will produce the same FA values.

In diffusion, forms of pulse sequences include spin-echo, stimulated-echo, and steady-state free precession (SSFP). A spin-echo pulse sequence is the most common method for producing MR imaging sensitive to diffusion. The diffusion-weighted stimulated echo sequence is important for tissues with short T_2 relaxation times (liver). It can be combined with reading techniques, such as echo-planar imaging (EPI) or spiral imaging. To mitigate the effects of subject motion and maintain a high signal-to-noise ratio (SNR), the EPI method is used to achieve fast image acquisition. Echo-planar imaging is vulnerable to artifacts such as ghosting, chemical shift, and distortions [26]. It has been shown that parallel imaging techniques to reduce echo train lengths minimize susceptibility-related EPI artifacts in DWI and improve image quality, particularly at a field strength of 3 T [27]. Echo-planar imaging, nevertheless, is constrained by noise and typically uses thicker slices compared to CE- T_1 imaging [3]. Theoretically, stimulated echoes have just half the signal compared to spin echoes. Furthermore, rapid image formation is possible regarding the very short imaging of T_R SSFP, which has high sensitivity to flow and diffusion [28].

This review aims to describe advanced magnetic resonance imaging modalities and recent findings in the literature on the diagnostics of breast cancer in the early stages.

2. DWI in the Field of Diagnostic Breast Cancer

Diffusion (Brownian motion) is a term that refers to the arbitrary, tiny development of water and other small molecules due to thermal excitation. When diffusion is similar in every direction, it is isotropic and is denoted by a single diffusion coefficient (D) as follows:

$$D_{\text{isotropic}} = \begin{bmatrix} D_{xx} & 0 & 0 \\ 0 & D_{yy} & 0 \\ 0 & 0 & D_{zz} \end{bmatrix}$$

where ($D_{xx} = D_{yy} = D_{zz} = D$).

The signal intensities in DWI are:

$$S_{\text{DWI}} = \sqrt[3]{S_x S_y S_z} = S_0 \times e^{-b(D_{xx} + D_{yy} + D_{zz})/3} = S_0 \times e^{-b(\text{trace})/3} = S_0 \times e^{-b \cdot \text{ADC}}$$

where diffusion trace is expressed as $D_{xx} + D_{yy} + D_{zz}$ and average trace is ADC.

It is noteworthy that ADC in the breast (fibro-glandular tissue) is equal to $2.37 \times 10^{-3} \text{ mm}^2/\text{s}$ [29]. DWI can be obtained by placing two additional diffusion-sensitizing gradients on each side of a spin-echo sequence's 180° radiofrequency (RF) pulse. The diffusion weighting's magnitude is achieved as follows:

$$b = \gamma^2 G^2 \delta^2 \left(\Delta - \frac{\delta}{3} \right)$$

where γ is the gyromagnetic ratio, G is the magnitude of the diffusion sensitizing gradients, δ is the temporal duration of each gradient, and Δ is the time interval between the application of the gradients.

The ADC value is a function of the chosen b values. Thus, when greater b values are used, the ADC values become smaller, and the specificity of DWI can be increased by higher b values [13]. Images with a high b value exhibit a decreased SNR and higher image distortion [30].

In a study, Dorrius et al. evaluated the b value's effect and the contrast's pre-admission on the diagnostic accuracy using 1.5 T for breast DWI. According to their research, $b = 0$ accompanied by $1000 \text{ s}/\text{mm}^2$ is suggested to distinguish between normal and cancer tissues when time constraints allow only diffusion images obtained at a couple of amounts of b [16]; however, high b -value DWI accompanied by conventional MRI sequences can facilitate the diagnosis closely to DCE-MRI for breast cancer detection [31]. In many studies, it has been hypothetically shown that the ideal pair amounts of b to alleviate noise effects are in the range of 0 to $1000 \text{ s}/\text{mm}^2$ in the brain (with moderately slow diffusion), while 0 and $800 \text{ s}/\text{mm}^2$ are ideal in most low-water-content tissue such as breast [32,33]. Signal decay varies according to the baseline T_2 signal in benign and malignant breast cancer, as indicated in Figure 1.

Diffusion-weighted imaging signal is generally T_1 - and T_2 -weighted, and higher-water-content lesions may have a high brilliance on DWI pictures; however, this is because of their exceptionally high T_2 signal and is not associated with diffusion (T_2 shine-through effect). One way to deal with this issue is to measure the ADC, which relies solely on diffusion [34]. Moreover, increasing the number of excitations in a fast DWI protocol has no diagnostic value according to Mori et al. They found no meaningful differences between one and four excitations in terms of lesion detectability or mean and minimum ADC value [35].

The common readout for breast DWI is single-shot EPI sequences, and readout segmented multi-shot EPI sequences. Echo planar imaging sequences are fast and insensitive to move, but they are vulnerable to geometric distortions that are most noticeable in the direction of phase encoding, leading to lower precision of quantification [36]. Moreover, EPI undergoes blurring due to T_2^* decay during readout. To decrease distortions, using some approaches such as high receiver bandwidth, parallel imaging, readout-segmented multi-

shot EPI sequences [37], combined EPI acquisitions with integrated dynamic shimming [38], and reduced field of view (rFOV) [39] can be helpful.

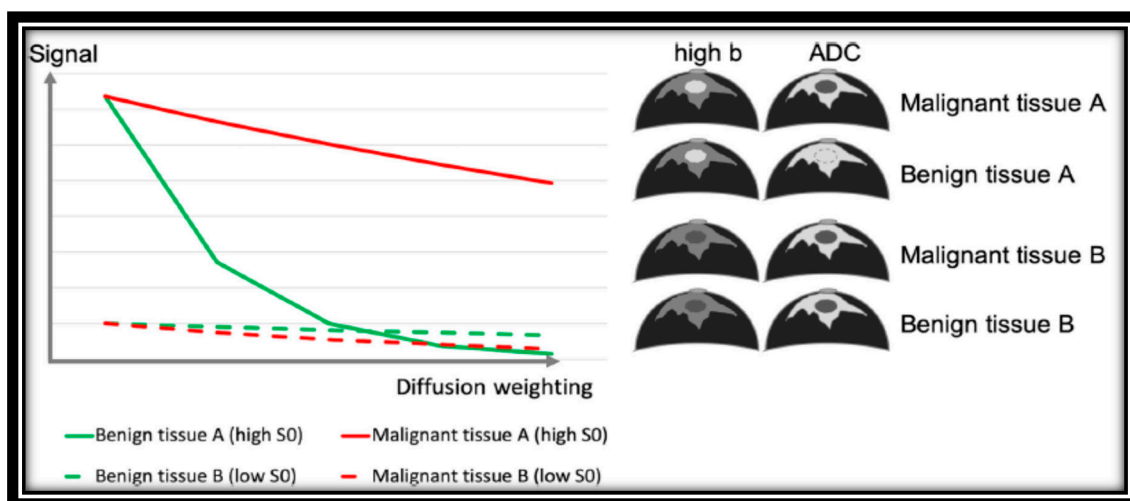


Figure 1. Signal decay of benign and malignant breast tissue in diffusion weighting imaging depending on baseline T₂ signal [33]. “Reprinted with permission from Ref. [33]. 2020, springer”. More details on “Copyright and Licensing” are available via the following link: <https://link.springer.com/article/10.1007/s00330-019-06510-3>.

In parallel imaging, the k-space lines are omitted, and the distance between them is increased.

Parallel imaging is widely used at a magnetic field strength of 3 Tesla since susceptibility effects are increased at greater field strengths. However, applying them at magnetic field strength 1.5 Tesla provides other advantages, such as increasing the number of slices for the same T_R and decreasing acquisition time. Although parallel imaging can reduce artifacts by decreasing the length of the echo train and hence reducing the T₂* blurring, it is constrained by the hardware of the RF coil [40].

In rFOV, sharp images of a target region can be obtained by decreasing the matrix size, resulting in reduced susceptibility artifacts and higher spatial resolution, with the tradeoff of increased acquisition time, compared to single-shot EPI DWI. The depiction of lesion boundaries and heterogeneity partitioned from the encompassing fibro-glandular or adipose tissue can be troublesome with conventional EPI [7]. However, the latest research on breast imaging with rFOV DWI has demonstrated that the lesion visibility is increased, image quality is improved, and high resolution is obtained in comparison to images acquired with conventional bilateral DWI, representing them as a viable alternative of DCE-MRI in breast cancer patients [41].

By obtaining k-space in some segments, multi-shot methods often aim to decrease the length of the echo train. In this regard, Baxter et al. (2019) compared multi-shot DWI using multiplexed sensitivity encoding with conventional single-shot EPI-DWI. According to their study, ADC indicates a low variation coefficient (<2%) between single-shot EPI-DWI and multi-shot segmented EPI technique (multiplexed sensitivity encoding (MUSE-DWI) permutations), which was obtained by using the phantom. ADC values determined by MUSE were significantly lower in malignant lesions than single-shot EPI. Their study compared ADC and normalized ADC = $\left(\frac{ADC_{\text{lesion}}}{ADC_{\text{tissue}}}\right)$ variations using the phantom variation coefficient and a paired t-test on the studied patients. Their result showed that normalized ADC values were not significantly different. They also stated that the quality of DWI breast images obtained by MUSE could be improved in comparison to single-shot EPI [40].

3. Comparison of DWI with Other Modalities

Generally, breast cancer can be examined with various techniques such as ultrasound, mammography, perfusion, and diffusion. According to many cohort and systematic studies, the sensitivity of MRI is higher than mammography, ultrasound, and a combination of ultrasound and mammography [42–46].

Many studies have shown that MR imaging has 91–100% sensitivity, and the specificity of DCE-MRI is about 37–97% [43,47]. Dynamic contrast enhancement MRI has disadvantages, such as a high cost, and cannot be applied to renal dysfunction patients. Based on the literature, among these techniques, DWI helps distinguish between benign and malignant breast lesions [48,49].

In a study, Yabuuchi et al. [5] compared mammography, DCE-MRI, and a combination of diffusion-weighted and T₂-weighted imaging (DWI + T₂WI) to detect non-palpable breast cancer in asymptomatic women. As indicated in Figure 2, the lesion was not visible on two-view mammography. The mass was enhanced on post-contrast MRI, easily identified on MIP. The mass appears to have a high signal on DWI and low ADC on DWI and ADC maps. According to their report, DWI + T₂WI showed a higher area under the curve (AUC) (AUC = 0.73; sensitivity = 50%) than mammography alone (AUC = 0.64; sensitivity = 40%), but lower than DCE-MRI (AUC = 0.93; sensitivity = 86%). Moreover, a combination of mammography and DWI + T₂WI showed greater sensitivity (69%) than mammography alone (40%). Having said that, false-positive outcomes using MRI images in high-risk lesions are substantially different from false-positive findings by mammography in low-risk lesions, according to Kuhl et al. [50].

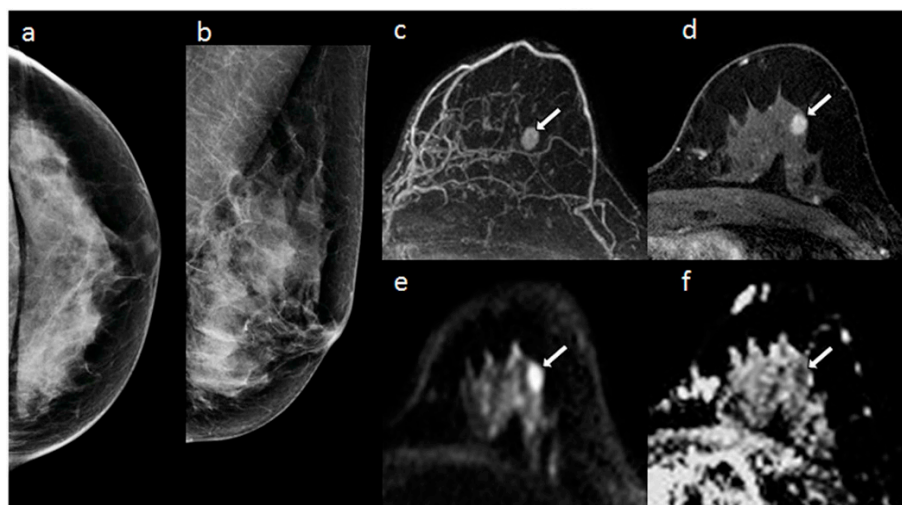


Figure 2. A 58-year old woman with dense breasts and invasive ductal carcinoma. (a) X-ray mammogram CC view and (b) MLO view, (c) DCE maximum intensity projection, (d) axial T₁-weighted fat saturated DCE-MRI, (e) axial DWI, and (f) ADC map [5]. “Reprinted with permission from Ref. [5]. 2011, springer”. More details on “Copyright and Licensing” are available via the following link: <https://link.springer.com/article/10.1007/s00330-010-1890-8>. White arrows indicated lesion in the images.

Zhang et al. conducted a study to determine which DCE-MRI, DWI, and T₂-weighted image descriptors are most closely related to breast cancer diagnosis. Their study set the b value to 50 and 850 s/mm². On DWI, malignant lesions exhibited a significantly lower average ADC mean (0.90×10^{-3} mm²/s) than benign lesions (1.43×10^{-3} mm²/s). They showed that DCE-MRI and DWI quantitative and qualitative variables are included in a multi-parametric MRI modality for breast cancer diagnosis. Indeed, they noted that models using the American College of Radiology (ACR) provide high diagnostic accuracy. Breast Imaging Reporting and Data System (BI-RADS) descriptors of margins and enhancement kinetics on DCE-MRI and ADC mean (either with DWI using a cutoff value or

as a continuous variable) are mainly connected with a breast cancer diagnosis. Conventional T₂-weighted imaging did not remarkably contribute to breast cancer diagnosis [51].

In 2019, Egnell et al. conducted a study to determine how stromal collagen fibers correlate with in vivo DWI. They used a high *b* value scheme to assess the association between collagen content and ADC and the signal fractions of the bi-exponential model. According to their study, collagen content is associated with the quick signal fraction and ADC values. They also found that the cellular content was inversely associated with the short signal fraction and ADC and varied between malignant, benign, and normal [52].

4. Different Models in DWI

As indicated in the literature, numerous models are available for extracting quantitative characteristics from images such as mono-exponential, intravoxel incoherent motion (IVIM) or bi-exponential, diffusion kurtosis imaging (DKI), stretched-exponential, Padé exponent (PE), statistical, and fractional-order calculus.

For instance, mono-exponential is the simplest model, often helpful if diffusion is analyzed on a voxel level [53]. The equation of mono-exponential is as follows:

$$S_b = S_0 \times e^{-b \cdot \text{ADC}}$$

where S_b is the signal intensity with *b* value, and S_0 is the signal intensity with $b = 0$.

The signal for the bi-exponential IVIM model is given by:

$$S_b = S_0 (1 - f) \cdot e^{-b \cdot D} + f \cdot e^{-b(D + D^*)}$$

where *D* is true diffusivity, *f* is Perfusion fraction, and D^* is pseudo-diffusivity.

In this model, which incorporates both diffusion and perfusion, *f* can be calculated as follows:

$$F = \frac{S(b = 0) - S_{\text{int}}}{S(b = 0)}$$

where S_{int} can be assessed by a mono-exponential fit applied to the high *b* value range.

The equation of diffusion kurtosis is:

$$S = S_0 \exp(-b \cdot D_K + \frac{1}{6} b^2 D_K^2 \cdot K)$$

where *K* is the kurtosis coefficient and D_K is the kurtosis corrected diffusion coefficient.

Anisotropic Gaussian diffusion is assumed by both the mono-exponential and IVIM models. Meanwhile, non-Gaussian diffusion can be considered by the kurtosis model.

The signal of the stretched-exponential model is as follows:

$$S_b = S_0 \times e^{-(b \cdot \text{DDC})^\alpha}$$

where DDC (distributed diffusion coefficient) is a measure of signal decay rate with *b* values and α is the heterogeneity index between 0 and 1. Figure 3 provides an example of a fitting by the DDC model.

The equation of the Padé exponent (PE) is given by:

$$S = S_0 \cdot e^{\frac{-D_p \cdot b}{1 + \delta_p \cdot b}}$$

where δ_p is quantified non-Gaussianity and D_p is diffusivity.

The signal of the statistical model is obtained by the following equation:

$$S = S_0 \cdot \frac{1 + \varphi\left(\frac{\text{ADC}_{\text{peak}}}{\sigma\sqrt{2}} - \frac{b\sigma}{\sqrt{2}}\right)}{1 + \varphi\left(\frac{\text{ADC}_{\text{peak}}}{\sigma\sqrt{2}}\right)} e^{-b \cdot \text{ADC}_{\text{peak}} + \frac{1}{2} b^2 \sigma^2}$$

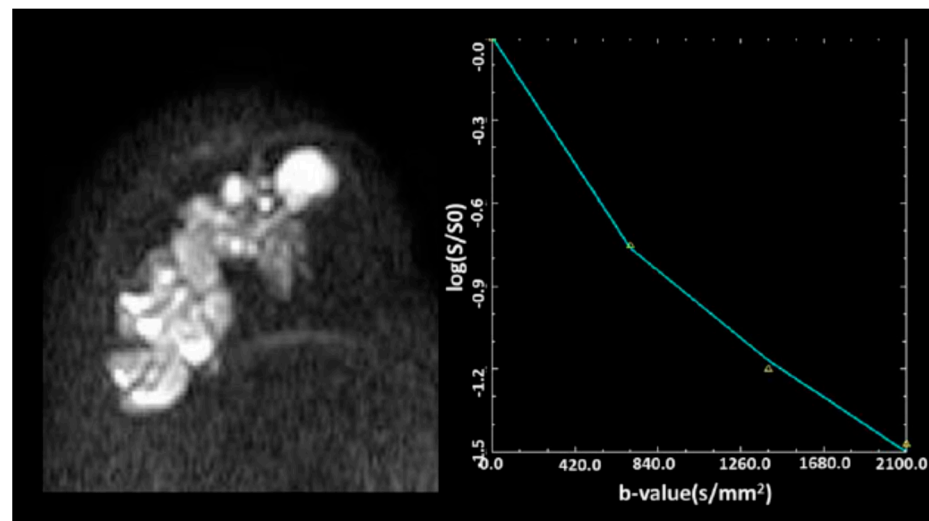


Figure 3. At the b value of 700–2100 s/mm^2 , the signal decay is slower, indicating a multi-exponential signal decay pattern of breast carcinoma [54]. Reprinted with permission from Ref. [54]. 2018, Wiley Online Library". More details on "Copyright and Licensing" are available via the following link: <https://onlinelibrary.wiley.com/doi/abs/10.1002/jmri.25904>.

The equation of fractional order calculus is as:

$$S = S_0 \cdot e^{-(b^* \cdot D^*)^\beta}$$

$$b^* = (\gamma G_d \delta)^2 \left(\Delta - \frac{2\beta - 1}{2\beta + 1} \delta \right)$$

$$D^* = D^{\frac{1}{\beta}} \mu^{2(1 - \frac{1}{\beta})} \left(\Delta - \frac{2\beta - 1}{2\beta + 1} \delta \right)^{\frac{1}{\beta} - 1}$$

where G_d is the diffusion gradient amplitude, δ is the diffusion gradient pulse lobe duration, Δ is diffusion gradient pulse separation, D is the diffusion coefficient, b is the fractional-order derivative in space, and μ is a spatial parameter.

Igor Vidić et al. assessed different non-Gaussian representations of DWI signals for benign and malignant breast lesions in the b range of 200 to 3000 s/mm^2 . According to their study, diffusion signal models provided parameters with a high area under the curve ($\text{AUC} > 0.9$) for classifying benign and malignant lesions. In their reports, the highest AUC of 0.99 was achieved for f (bi-exponential), K (kurtosis), and 0.989 for D (fractional calculus). Additionally, non-Gaussian representations are required for fitting the DWI curve at high b values in breast lesions. Moreover, the single voxel analysis showed that the SNR provided high classification accuracy for the statistical and fractional calculus diffusion model. Meanwhile, the other non-Gaussian representations gave lower classification accuracy than the mono-exponential model [55].

Bedair et al. evaluated the response of breast tumors to neoadjuvant chemotherapy at a field strength of 3 T using mono-exponential, bi-exponential, and stretched-exponential models. Mean diffusion coefficients at pretreatment revealed substantial variations between the analyzed groups in their study. The percentage rise in ADC and DDC had substantial disparities between responders and non-responders, and stretched-exponential parameters showed excellent repeatability. They also showed that DWI is sensitive to early treatment changes in breast cancer utilizing non-mono-exponential models, and the stretched-exponential model can be used to monitor such changes [56].

In another work, Suo et al. examined breast lesion differentiation using mono-exponential, bi-exponential, stretched-exponential, and kurtosis models. All diffusion measurements showed substantial variations in their findings, except for mean diffusivity between benign and malignant lesions. Moreover, no significant variations between ADC

and non-mono-exponential diffusion parameters were observed in areas under the ROC curves, except for D_f (bi-exponential) and α (stretched-exponential), the AUCs of which were substantially lower than the ADC AUC for differentiating benign from malignant lesions. D_f was strongly correlated with lymph node metastasis and Ki-67 expression in patients with invasive breast cancer. Moreover, ADC, D_s (bi-exponential), f (bi-exponential), DDC (stretched-exponential), and mean diffusivity were highly correlated with estrogen receptor status. Overall, they claimed that multi-parametric DWI is associated with breast lesions' pathological outcomes and prognostic factors [57].

5. DWI in Treatment Evaluation of Breast Cancer

There are many uses for treatment planning in DWI that can help detect and characterize tumors and predict and evaluate therapy response in malignancies, wherein hyper-cellular metastases and fibrosis-restricted diffusion is mainly observed [9]. It is specified that tumors with a more significant mean ADC pretreatment are more likely to be necrotic [58], and may therefore include more hypoxic areas. Additionally, diffusion continues to increase during radiotherapy because of cell membrane destruction and treatment-induced cell death [59,60].

Mammography, sonography, and MRI can be used to check the size changes after neoadjuvant chemotherapy (NAC). MRI may be an effective strategy for studying the impact of NAC, and it may be accommodating to choose the extent of surgery. In this regard, the sensitivity of MRI in the initial staging of breast cancer and detecting the residual cancerous tissues following neoadjuvant chemotherapy was reported to be higher in comparison to breast-specific gamma imaging (83.9% to 76.8%), while their specificity was comparable, with 58.8% and 70.6%, respectively [61]. The same results were acquired in the study by Lee et al., where the detectability rate of MRI for breast cancer recurrence was considerably higher in contrast to ultrasound imaging [62]. However, in another study to investigate the detection efficacy of MRI in breast cancer patients for axillary lymph node metastasis, post-neoadjuvant chemotherapy, its sensitivity, specificity, and positive and negative predictive value fell short compared to ultrasound imaging [63]. Moreover, the role of PET/CT for the expectation of pathologic reaction is not predominant in MRI [64]. Therefore, there is a tendency to use MRI.

Chu et al. conducted a meta-analysis to determine the diagnostic efficiency of DWI in breast cancer to monitor pathological responses to neoadjuvant chemotherapy. In this study, the pooled weighted values had sensitivity of 0.88, specificity of 0.79, a positive likelihood ratio of 4.1, a negative likelihood ratio of 0.16, and a diagnostic odds ratio of 26. The area under the receiver operator characteristic curve was 0.91. In the subgroup analysis, the pooled specificity of change in the ADC subgroup was higher than that in the pretreatment ADC subgroup [65]. The correlation of ADC and FA (fractional anisotropy) was also examined by others, and the results indicated that the ADC and FA values of malignant lesions were statistically lower than those of benign lesions, and the combined DTI and FT (fiber tractography) sensitivity, specificity, and accuracy were comparable to DCE-MRI (96%, 90%, and 94%, respectively) [66,67].

To direct treatment decisions, precise loco-regional staging and preoperative evaluation of breast cancer are considered crucial [68]. In 2021, Hashem et al. assessed the role of DCE and DWI in the preoperative staging of breast cancer. This study showed that DCE could detect the ductal carcinoma in situ (DCIS) component of the malignant lesions and give better tumor size and hence superior staging outcomes over sono-mammography. Moreover, they stated that qualitative DWI could be accompanied by ultrasonography to better assess the axillary nodal status. Both combinations enable the preoperative loco-regional staging of malignant breast disease to be effective and precise [69].

Ergul et al. compared the utility of 18F-fluorodeoxyglucose positron emission tomography/computed tomography (FDG PET/CT), DCE, and DWI and sentinel lymph node biopsy (SNB) in the diagnosis of axillary metastatic lymph nodes in early-stage breast cancer (ESBC) patients. According to these researchers, DCE-MRI provides relatively higher

sensitivity than FDG PET/CT when investigating ESBC multifocality. They also suggested that FDG PET/CT has higher sensitivity and reliability than both DCE-MRI and DWI, and FDG PET/CT data will direct a selective SNB and axillary lymph node dissection (ALND) scheduling decision [70].

6. DTI in the Diagnosis of Breast Cancer

When diffusion in specific directions is more than in other directions, it is called anisotropic. In anisotropic diffusion, we cannot use a single diffusion coefficient; instead, we need to use a diffusion tensor.

$$D = \begin{bmatrix} D_{xx} & D_{xy} & D_{xz} \\ D_{yx} & D_{yy} & D_{yz} \\ D_{zx} & D_{zy} & D_{zz} \end{bmatrix}$$

DTI assesses water diffusion in a minimum of six directions. Parameters of DTI are ADC or mean diffusivity (MD), fractional anisotropy (FA), mean axial diffusivity λ_1 , mean radial diffusivity $(\lambda_2 + \lambda_3)/2$, and empirical difference $[\lambda_1 - \lambda_3]$.

The equation of ADC or MD is written as follows:

$$\frac{\lambda_1 + \lambda_2 + \lambda_3}{3}$$

FA is given by:

$$\frac{\sqrt{3}}{\sqrt{2}} \times \frac{\sqrt{(\lambda_1 - \text{ADC})^2 + (\lambda_2 - \text{ADC})^2 + (\lambda_3 - \text{ADC})^2}}{\sqrt{(\lambda_1^2 + \lambda_2^2 + \lambda_3^2)}}$$

Comparing DWI with DCE shows that DWI is faster than DCE [3]. Moreover, DCE has false-positive results and unnecessary biopsies. Other studies have shown that DWI will enhance the accuracy of breast cancer diagnosis and characterization. On the other hand, DTI is an improvement of conventional DWI that quantifies anisotropy by evaluating water motion in six or more directions in addition to ADC [29,71–73]. Consequently, ADC is an essential diffusion factor for determining the difference between benign and malignant breast tumors (lighter on DWIs and darker on ADC maps relative to standard fibro-glandular tissue). At the same time, anisotropy measures can help further characterize the microstructure and microenvironment of the tumor [74].

Tsougos et al. evaluated DTI for differentiating breast tumors by setting b values to 0 and 600 s/mm². The mean ADC value of malignant and benign lesions was $1.06 \times 10^{-3} \pm 0.24$ mm²/s and $1.54 \times 10^{-3} \pm 0.22$ mm²/s respectively, whereas it was $1.77 \times 10^{-3} \pm 0.20$ mm²/s for normal tissue. They reported that ADC measurements had lower malignant lesions values than the benign and normal breast [4].

Changes in the DTI parameters were evaluated by Scaranelo et al. [75] before and after Gd (gadolinium) administration. They observed all breast cancers in the DDC (distributed diffusion coefficient) λ_1 maps before and after administration of Gd-based contrast agents (GBCAs). The mean size of cancer extracted from λ_1 maps before administration of GBCAs remained statistically indistinguishable from the size determined following administration. The cancers showed remarkably lower DDCs, mean diffusivity, and intensity after GBCA administration and no alteration in maximal anisotropy in comparison with prior GBCA administration. For all parameters, except for λ_3 , the mean AUC values before and after GBCA administration did not vary considerably [75].

Nissan et al. (2020) [76] compared the influence of lactation on breast cancer conspicuity using DCE with DTI parametric maps. They showed a reduction in the contrast-to-noise ratio of breast cancer to DCE values compared to non-lactating patients. DTI parameters of λ_1 , λ_2 , λ_3 , mean diffusivity, and $\lambda_1 - \lambda_3$ significantly declined among lactating patients. Additionally, FA significantly increased in breast cancer associated with pregnancy compared to the normal lactating parenchyma region of interest. The contrast-to-noise in eigenvalues (λ_1 , λ_2 , λ_3) and mean diffusivity were substantially superior to DCE in the lactating cohort [76].

The diagnostic performance of DTI parameters is controversial in the literature. In one study by Onaygil et al., breast cancer diagnostic factors were assessed. According to their results, in addition to the ability of this method to identify malignant breast lesions, DTI increased the sensitivity of the traditional 3 T breast MRI system and showed a correlation with estrogen receptor (ER) and Ki-67 biomarkers. However, in another study conducted by Abdelhady et al., the sensitivity and specificity of DTI in differentiating benign breast lesions from malignant tissue were lower than those of DWI [77]. Overall, DTI was proved to be a potential instrument for differential diagnosis to aid DCE-MRI and assess molecular subtypes in breast cancer [78].

7. DTI in Treatment Evaluation of Breast Cancer

The potential of DTI and DCE to monitor response to neoadjuvant chemotherapy was assessed by Edna Furman-Haran et al. [79]. In their study, the cancers scanned before neo-adjuvant chemotherapy in the three directional diffusion coefficients, λ_1 , λ_2 , and λ_3 , and the mean diffusivity. They found that the maximal anisotropy and l1–l3 had lower levels in cancerous locations than normal tissue, which were reported in other studies, as well [80,81]. They also reported an increase in the eigenvalues and mean diffusivity in response to neoadjuvant chemotherapy. Indeed, they showed that DTI can monitor alterations in the size and diffusion tensor parameters of breast cancer in response to neoadjuvant chemotherapy with an accuracy comparable to that of DCE [79].

Wilmes et al. investigated the prognostic importance of tumor metrics obtained from DTI. In this study, DTI and CE-MRI were carried out prior to treatment and after three cycles of taxane-based therapy (early treatment). According to the obtained results of tumor pretreatment, ADC was notably lower in the complete pathological response (pCR) than in the non-pCR group. At initial treatment, patients with pCR had a considerably more significant change in tumor eigenvalues (λ_1 , λ_2 , λ_3) and ADC than those without pCR. Moreover, they observed that while there was a weak correlation in early percentage changes in tumor FA with pCR, the correlation with the final improvement in tumor volume with pCR is related to therapy [82].

Numerous studies have mentioned the ability of neurotoxicity of chemotherapy for breast cancer. For instance, Menning et al. assessed chemotherapy's adverse effects on white matter. They examined this issue before and six months after chemotherapy, using matched intervals for the unexposed groups. Based on voxel analysis, their study did not indicate an effective chemotherapy with and without endocrine treatment on the integrity of white matter. Region of interest evaluation showed chemotherapy's adverse effects with and without endocrine therapy by establishing a more significant decline in white matter (WM) integrity in the superior longitudinal fasciculus and corticospinal tract in breast cancer patients receiving systemic treatment than breast cancer patients who did not need chemotherapy [83].

8. Amide Proton Transfer-Weighted Imaging in Breast Cancer Diagnosis

As a molecular imaging technique, amide proton transfer-weighted imaging (APTWI) measures the concentration of unbound proteins and polypeptides in tissue with no need for extrinsic contrast agents. Instead of relying on water molecule diffusion within tissues, APTWI's capacity to represent lesion information is achieved by monitoring the chemical rate of exchange between water and amide protons [84]. A study on the application of APTWI to assess breast lesions recently commenced. While several research findings have evaluated the utility of APTWI in tumor grading, cell proliferation [85], and its importance in treatment-related lymphedema therapy [86], few studies have examined APTWI's effectiveness in diagnosing benign and malignant lesions and the connection among its parameters and prognostic factors [87]. Meng et al. attempted to evaluate the roles of diffusion kurtosis imaging (DKI) and APTWI in distinguishing benign and malignant breast lesions and examine the correlation coefficients between the obtained parameters and breast cancer prognostic factors to develop novel concepts for breast cancer diagnosis, treatment,

and prognostic assessment. The results indicated that the DKI and APTWI both offer useful information about the characteristics of breast lesions, apparent kurtosis coefficient (K_{app}), non-Gaussian diffusion coefficient (D_{app}), and magnetization transfer ratio asymmetry (MTR_{asym} (3.5 ppm)), which are all viable variables for determining the microstructure of tissue, and overall, DKI was found to be superior to APTWI in discriminating benign from malignant breast lesions for three main reasons. Firstly, the discrepancies in water molecule diffusion in cancer cells are larger than the protein and polypeptide composition changes. Secondly, the key contributors to alterations in the protein and polypeptide content of the microenvironment remain unknown. Finally, the APTWI technique is still being developed, and scanning precision could be improved [88].

9. Diffusion Kurtosis Imaging in Breast Cancer Diagnosis

While pure liquids and gels exhibit a Gaussian distribution of diffusion, obstacles induced by complicated tissue constructs effectively alter the probability distribution of diffusion. Kurtosis is the statistical term for assessing the true probability distribution within tissue. By obtaining supplementary images with a higher b-value (where b is an operator-defined parameter corresponding to the strength and duration of diffusion in imaged tissues), on the order of $b = 1000\text{--}3000 \text{ s/mm}^2$ and at least 15 diffusion gradient directions, the diffusion kurtosis imaging method can trace numerous structures inside a single voxel, for example, crossing white matter fibers in the brain. In the case of breast imaging, diffusion kurtosis imaging is susceptible to intracellular structures such as membranes and organelles [61] and can offer a diffusion heterogeneity index sensitive to tumor microstructure in addition to a mean kurtosis map [62]. Notably, when the unsuppressed fat signal is corrected for, diffusion kurtosis analysis of the breast improves [63].

Diffusion kurtosis imaging (DKI), proposed by Jensen et al., is a beneficial diffusion imaging technique [89]. Compared to standard DWI, DKI considers the non-Gaussian diffusion of water molecules within tissues and incorporates a fourth-order three-dimensional tensor into the structure of its model; as a result, DKI can approximate the microstructural heterogeneity of tissues [90]. Several researchers have explored the correlation between relevant DKI parameters and prognostic factors such as heterogeneous malignancy, discrepancies in pathological characteristics and grade, expression of ER and PR, and tumor diameter [57,91], but no conclusive findings were attained.

10. Magnetic Resonance Spectroscopy

Magnetic resonance spectroscopy (MRS) is a noninvasive imaging modality often implemented to assess the metabolic data inside a targeted tissue by revealing the spike in specific metabolites, such as total choline (tCho). Increased tCho levels have been identified in malignant tumors, including breast cancer, attributed to the increased cell membrane turnover of neoplastic processes. Numerous studies have shown that incorporating MRS into routine breast MR examinations enhances diagnostic performance and decreases the probability of needless biopsies. MRS has sufficient sensitivity of 71–74% and specificity of 78–88% for differentiating benign from malignant lesions [92–94]. Numerous findings have established a link between raised tCho concentrations and biologically aggressive cancer characteristics attributed to high grade, large dimensions, and a high Ki67 proliferation rate [95]. In addition to tCho, MRS is often used to identify and detect other metabolites, such as lipids, as abnormalities in lipid metabolism have been linked to cancer development in recent years. Thakur et al. established the diagnostic and prognostic utility of MRS by indicating that quantitative in vivo MRS analysis of the lipid metabolism of breast lesions enabled the detection of malignancies and subtypes of breast cancer [96]. Incorporating the lipid analysis into the tCho peak in MRS to detect breast cancer showed higher sensitivity compared to the situation where only one of them was measured [97].

11. Perspectives (Future Directions)

This review provides a broad overview and comparison of various MR imaging methods, including DCE, DWI, and DTI, for breast cancer diagnosis. As mentioned earlier, MRI is more sensitive than mammography and sonography [42,43]. DCE has limitations compared to other MRI models, such as high cost and inability to use in patients with renal dysfunction. However, comparisons of DCE, DWI, and T₂-weighted techniques have shown that the use of DCE and DWI in diagnosing breast cancer is beneficial [48,49,98], but T₂-weighted MRI cannot be significantly helpful [51]. Indeed, DWI plus T₂-weighted MRI are less sensitive than DCE [5]. In addition to the diagnostic context, DWI has been evaluated in therapy planning, such as the evaluation of tumor response to treatment.

Tables 1 and 2 summarize the essential criteria of different MRI methods for breast cancer diagnosis. As shown in Table 1, ADC has the most critical diffusion parameter in differentiating between benign and malignant breast lesions, while anisotropy measures can help further characterize the tumor [74]. In malignant lesions, the eigenvalues ($\lambda_1, \lambda_2, \lambda_3$) and mean diffusivity or ADC due to diffusion limit should be less than in benign lesions and normal breasts. Moreover, ADC in malignant lesions was lower than in benign lesions and normal breasts. It has also been shown that in lactating patients, the values of $\lambda_1, \lambda_2, \lambda_3$, mean diffusivity, and $\lambda_1-\lambda_3$ are significantly reduced. Moreover, FA is significantly increased in breast cancer associated with pregnancy compared to normal lactating parenchyma [76]. DTI study in therapy has also shown that eigenvalues and mean diffusivity increase in response to neoadjuvant chemotherapy [79].

Table 1. The most important DTI characteristics for breast cancer.

Ref.	λ_1	λ_2	λ_3	MD	FA	$\lambda_1-\lambda_3$
Noam Nissan et al. [76] in pregnancy-associated breast cancer	1.17 ± 0.11	0.95 ± 0.11	0.74 ± 0.11	0.95 ± 0.11	0.25 ± 0.05±	0.43 ± 0.07
Haran et al. [79] (median % change responders)	55.7 (43.6–77)	55.4 (42.3–74.2)	61.5 (41.3–81.0)	55.6 (42.4–71.8)	1.3 (214.3–20.8)	55.4 (42.4–100.1)
Onaygil et al. [78]	1.91 ± 0.30 * 1.27 ± 0.19 **	1.68 ± 0.28 * 1.01 ± 0.20 **	1.46 ± 0.27 * 0.81 ± 0.24 **	1.68 ± 0.27 * 1.03 ± 0.19 **	0.14 ± 0.05 * 0.24 ± 0.14 **	0.45 ± 0.17 * 0.48 ± 0.25 **

$\lambda_1, \lambda_2, \lambda_3$: eigenvalues, MD: mean diffusivity, FA: fractional anisotropy, $\lambda_1-\lambda_3$: empirical difference, ADC: apparent diffusion coefficient, *: benign, **: malignant.

Table 2. The most important DWI characteristics for breast cancer.

Ref.	(ADC: ×10 ³ mm ² /s) Malignant	(ADC: ×10 ³ mm ² /s) Benign
Egnell et al. [52] b-values (0, 200, 600, 1200, 1800, 2400, 3000) s/mm ²	=1.04 (0.96–1.20)	=1.75 (1.51–1.86)
Pereira et al. [3] b-values (0, 250, 500, 750, and 1000)	0.907	1.45
Sinha et al. [29]	1.36 ± 0.36	2.01 ± 0.46

$\lambda_1, \lambda_2, \lambda_3$: eigenvalues, MD: mean diffusivity, FA: fractional anisotropy, $\lambda_1-\lambda_3$: empirical difference, ADC: apparent diffusion coefficient.

Many studies have confirmed that DCE can determine tumor size and can have better staging than sono-mammography. The combination of DWI and ultrasound can also be valuable and accurate for the preoperative loco-regional staging of malignant tumor lesions [98]. In addition to examining the effectiveness of DWI in breast cancer, the significance of DTI has been considered. A comparison of DTI and DCE in the evaluation of tumor response to treatment has shown that before treatment, the amount of ADC in patients with pCR is less than in non-pCR patients. In early treatment in patients with pCR, the most changes in eigenvalues and ADC compared to non-pCR patients are observed [82].

Currently, because of the diversity in MRI models and instruments, only a few of them are available in clinics. With the development in MR instruments and technology, it is predicted that new MRI systems and methods will achieve the most advancement. Although many MR instruments and techniques are available, all have their limitations. In the future, with the development of instruments and advances in MR imaging modalities, software, image processing, and health management, they will provide a new platform for cancer diagnosis. These developments would also allow clinicians to predict better treatment.

For medical students, radiologists, and researchers interested in cancer diagnosis and therapy, this review article could be helpful. The limitation of this article is that we could not access all newly published papers or cover every aspect of all recent findings on breast cancer diagnosis.

12. Conclusions

Dynamic contrast-enhanced MRI (DCE-MRI) has high sensitivity and changeable specificity for breast cancer. DWI and its characteristics can show tumor cell thickness and microstructure or microvasculature at the cellular level without contrast agents. Recent findings have confirmed that DTI as an MR imaging modality has the potential for differential breast cancer diagnosis and could aid DCE-MRI and assess molecular subtypes in breast cancer detection. The diagnostic performance of new advances may be helpful in DTI, DWI, and DCE-MRI parameters and can help in the diagnosis of breast cancer in the early stages. Overall, recent findings showed that DWI and DTI and their characteristics may facilitate earlier and more accurate breast cancer diagnosis and treatment.

Author Contributions: Conceptualization, D.S.-G.; Methodology, D.S.-G., F.A., H.N. and M.G.; Validation, D.S.-G.; Investigation, D.S.-G., F.A., H.N., M.G. and S.S.G.; Resources, D.S.-G.; Data Curation, D.S.-G., F.A. and H.N.; Writing—Original Draft Preparation, F.A. and H.N.; Writing—Review and Editing, D.S.-G., M.G. and S.S.G.; Supervision, D.S.-G.; Project Administration, D.S.-G.; Funding Acquisition, D.S.-G. All authors have read and agreed to the published version of the manuscript.

Funding: This study was funded by Isfahan University of Medical Sciences, Isfahan, Iran (grant number 3400413).

Institutional Review Board Statement: This article does not contain any studies with human participants or animals performed by any of the authors.

Data Availability Statement: The data presented in this study are available on request from the corresponding author.

Conflicts of Interest: The authors declare that they have no conflict of interest.

References

1. Khaniabadi, P.M.; Shahbazi-Gahrouei, D.; Aziz, A.A.; Dheyab, M.A.; Khaniabadi, B.M.; Mehrdel, B.; Jameel, M.S. Trastuzumab conjugated porphyrin-superparamagnetic iron oxide nanoparticle: A potential PTT-MRI bimodal agent for herceptin positive breast cancer. *Photodiagnosis Photodyn. Ther.* **2020**, *31*, 101896. [[CrossRef](#)] [[PubMed](#)]
2. Shahbazi-Gahrouei, D.; Khaniabadi, P.M.; Khaniabadi, B.M.; Shahbazi-Gahrouei, S. Medical imaging modalities using nanoprobes for cancer diagnosis: A literature review on recent findings. *J. Res. Med. Sci. Off. J. Isfahan Univ. Med. Sci.* **2019**, *24*, 38. [[CrossRef](#)] [[PubMed](#)]
3. Pereira, F.P.A.; Martins, G.; de Oliveira, R.d.V.C. Diffusion magnetic resonance imaging of the breast. *Magn. Reson. Imaging Clin.* **2011**, *19*, 95–110. [[CrossRef](#)] [[PubMed](#)]
4. Tsougos, I.; Bakosis, M.; Tsivaka, D.; Athanassiou, E.; Fezoulidis, I.; Arvanitis, D.; Vassiou, K. Diagnostic performance of quantitative diffusion tensor imaging for the differentiation of breast lesions at 3 T MRI. *Clin. Imaging* **2019**, *53*, 25–31. [[CrossRef](#)] [[PubMed](#)]
5. Yabuuchi, H.; Matsuo, Y.; Sunami, S.; Kamitani, T.; Kawanami, S.; Setoguchi, T.; Sakai, S.; Hatakenaka, M.; Kubo, M.; Tokunaga, E. Detection of non-palpable breast cancer in asymptomatic women by using unenhanced diffusion-weighted and T2-weighted MR imaging: Comparison with mammography and dynamic contrast-enhanced MR imaging. *Eur. Radiol.* **2011**, *21*, 11–17. [[CrossRef](#)] [[PubMed](#)]

6. Shahbazi-Gahrouei, D.; Khaniabadi, P.M.; Shahbazi-Gahrouei, S.; Khorasani, A.; Mahmoudi, F. A literature review on multi-modality molecular imaging nanoprobe for cancer detection. *Pol. J. Med. Phys. Eng.* **2019**, *25*, 57–68. [[CrossRef](#)]
7. Partridge, S.C.; Nissan, N.; Rahbar, H.; Kitsch, A.E.; Sigmund, E.E. Diffusion-weighted breast MRI: Clinical applications and emerging techniques. *J. Magn. Reson. Imaging* **2017**, *45*, 337–355. [[CrossRef](#)]
8. Baliyan, V.; Das, C.J.; Sharma, R.; Gupta, A.K. Diffusion weighted imaging: Technique and applications. *World J. Radiol.* **2016**, *8*, 785. [[CrossRef](#)]
9. Malayeri, A.A.; El Khouli, R.H.; Zaheer, A.; Jacobs, M.A.; Corona-Villalobos, C.P.; Kamel, I.R.; Macura, K.J. Principles and applications of diffusion-weighted imaging in cancer detection, staging, and treatment follow-up. *Radiographics* **2011**, *31*, 1773–1791. [[CrossRef](#)]
10. Fohlin, H.; Bekkhus, T.; Sandström, J.; Fornander, T.; Nordenskjöld, B.; Carstensen, J.; Stål, O. RAB6C is an independent prognostic factor of estrogen receptor-positive/progesterone receptor-negative breast cancer. *Oncol. Lett.* **2020**, *19*, 52–60. [[CrossRef](#)]
11. Horvat, J.V.; Bernard-Davila, B.; Helbich, T.H.; Zhang, M.; Morris, E.A.; Thakur, S.B.; Ochoa-Albiztegui, R.E.; Leithner, D.; Marino, M.A.; Baltzer, P.A. Diffusion-weighted imaging (DWI) with apparent diffusion coefficient (ADC) mapping as a quantitative imaging biomarker for prediction of immunohistochemical receptor status, proliferation rate, and molecular subtypes of breast cancer. *J. Magn. Reson. Imaging* **2019**, *50*, 836–846. [[CrossRef](#)] [[PubMed](#)]
12. Suo, S.; Zhang, D.; Cheng, F.; Cao, M.; Hua, J.; Lu, J.; Xu, J. Added value of mean and entropy of apparent diffusion coefficient values for evaluating histologic phenotypes of invasive ductal breast cancer with MR imaging. *Eur. Radiol.* **2019**, *29*, 1425–1434. [[CrossRef](#)] [[PubMed](#)]
13. Iima, M.; Kataoka, M.; Kanao, S.; Onishi, N.; Kawai, M.; Ohashi, A.; Sakaguchi, R.; Toi, M.; Togashi, K. Intravoxel incoherent motion and quantitative non-Gaussian diffusion MR imaging: Evaluation of the diagnostic and prognostic value of several markers of malignant and benign breast lesions. *Radiology* **2018**, *287*, 432–441. [[CrossRef](#)] [[PubMed](#)]
14. Springer Jr, C.S. Using ¹H₂O MR to measure and map sodium pump activity in vivo. *J. Magn. Reson.* **2018**, *291*, 110–126. [[CrossRef](#)] [[PubMed](#)]
15. Baltzer, P.; Dietzel, M.; Vag, T.; Mieczyslaw, G.; Camara, O.; Kaiser, W. Diffusion weighted imaging-useful in all kinds of lesions? A systematic review. *Eur. Radiol.* **2009**, *19*, S765–S774.
16. Dorrius, M.D.; Dijkstra, H.; Oudkerk, M.; Sijens, P.E. Effect of b value and pre-admission of contrast on diagnostic accuracy of 1.5-T breast DWI: A systematic review and meta-analysis. *Eur. Radiol.* **2014**, *24*, 2835–2847. [[CrossRef](#)]
17. Benndorf, M.; Schelhorn, J.; Dietzel, M.; Kaiser, W.A.; Baltzer, P.A. Diffusion weighted imaging of liver lesions suspect for metastases: Apparent diffusion coefficient (ADC) values and lesion contrast are independent from Gd-EOB-DTPA administration. *Eur. J. Radiol.* **2012**, *81*, e849–e853. [[CrossRef](#)]
18. Leithner, D.; Moy, L.; Morris, E.A.; Marino, M.A.; Helbich, T.H.; Pinker, K. Abbreviated MRI of the breast: Does it provide value? *J. Magn. Reson. Imaging* **2019**, *49*, e85–e100. [[CrossRef](#)]
19. Kuhl, C.K.; Schrading, S.; Strobel, K.; Schild, H.H.; Hilgers, R.-D.; Bieling, H.B. Abbreviated breast magnetic resonance imaging (MRI): First postcontrast subtracted images and maximum-intensity projection—a novel approach to breast cancer screening with MRI. *J. Clin. Oncol.* **2014**, *32*, 2304–2310. [[CrossRef](#)]
20. Yamada, T.; Kanemaki, Y.; Okamoto, S.; Nakajima, Y. Comparison of detectability of breast cancer by abbreviated breast MRI based on diffusion-weighted images and postcontrast MRI. *Jpn. J. Radiol.* **2018**, *36*, 331–339. [[CrossRef](#)]
21. Shin, H.J.; Chae, E.Y.; Choi, W.J.; Ha, S.M.; Park, J.Y.; Shin, K.C.; Cha, J.H.; Kim, H.H. Diagnostic performance of fused diffusion-weighted imaging using unenhanced or postcontrast T1-weighted MR imaging in patients with breast cancer. *Medicine* **2016**, *95*, e3502. [[CrossRef](#)] [[PubMed](#)]
22. Bickelhaupt, S.; Laun, F.B.; Tesdorff, J.; Lederer, W.; Daniel, H.; Stieber, A.; Delorme, S.; Schlemmer, H.-P. Fast and noninvasive characterization of suspicious lesions detected at breast cancer X-ray screening: Capability of diffusion-weighted MR imaging with MIPs. *Radiology* **2016**, *278*, 689–697. [[CrossRef](#)] [[PubMed](#)]
23. Rajagopalan, V.; Jiang, Z.; Yue, G.H.; Radic, J.S.; Piro, E.P.; Wylie, G.R.; Das, A. A Basic Introduction to Diffusion Tensor Imaging Mathematics and Image Processing Steps. *Brain Disord* **2017**, *6*, 2. [[CrossRef](#)]
24. Wang, Y.; Zhang, X.-P.; Li, Y.-L.; Li, X.-T.; Hu, Y.; Cui, Y.; Sun, Y.-S.; Zhang, X.-Y. Optimization of the parameters for diffusion tensor magnetic resonance imaging data acquisition for breast fiber tractography at 1.5 T. *Clin. Breast Cancer* **2014**, *14*, 61–67. [[CrossRef](#)] [[PubMed](#)]
25. Koay, C.G.; Chang, L.-C.; Carew, J.D.; Pierpaoli, C.; Basser, P.J. A unifying theoretical and algorithmic framework for least squares methods of estimation in diffusion tensor imaging. *J. Magn. Reson.* **2006**, *182*, 115–125. [[CrossRef](#)] [[PubMed](#)]
26. Le Bihan, D.; Poupon, C.; Amadon, A.; Lethimonnier, F. Artifacts and pitfalls in diffusion MRI. *J. Magn. Reson. Imaging Off. J. Int. Soc. Magn. Reson. Med.* **2006**, *24*, 478–488. [[CrossRef](#)]
27. Bogner, W.; Gruber, S.; Pinker, K.; Grabner, G.; Stadlbauer, A.; Weber, M.; Moser, E.; Helbich, T.H.; Trattinig, S. Diffusion-weighted MR for differentiation of breast lesions at 3.0 T: How does selection of diffusion protocols affect diagnosis? *Radiology* **2009**, *253*, 341–351. [[CrossRef](#)]
28. Iima, M.; Honda, M.; Sigmund, E.E.; Ohno Kishimoto, A.; Kataoka, M.; Togashi, K. Diffusion MRI of the breast: Current status and future directions. *J. Magn. Reson. Imaging* **2020**, *52*, 70–90. [[CrossRef](#)]
29. Sinha, S.; Lucas-Quesada, F.A.; Sinha, U.; DeBruhl, N.; Bassett, L.W. In vivo diffusion-weighted MRI of the breast: Potential for lesion characterization. *J. Magn. Reson. Imaging: Off. J. Int. Soc. Magn. Reson. Med.* **2002**, *15*, 693–704. [[CrossRef](#)]

30. Geijer, B.; Sundgren, P.; Lindgren, A.; Brockstedt, S.; Ståhlberg, F.; Holtås, S. The value of b required to avoid T2 shine-through from old lacunar infarcts in diffusion-weighted imaging. *Neuroradiology* **2001**, *43*, 511–517. [[CrossRef](#)]
31. Ohlmeyer, S.; Laun, F.B.; Bickelhaupt, S.; Palm, T.; Janka, R.; Weiland, E.; Uder, M.; Wenkel, E. Ultra-High b-Value Diffusion-Weighted Imaging-Based Abbreviated Protocols for Breast Cancer Detection. *Investig. Radiol.* **2021**, *56*, 629–636. [[CrossRef](#)] [[PubMed](#)]
32. Amornsiripanitch, N.; Bickelhaupt, S.; Shin, H.J.; Dang, M.; Rahbar, H.; Pinker, K.; Partridge, S.C. Diffusion-weighted MRI for unenhanced breast cancer screening. *Radiology* **2019**, *293*, 504–520. [[CrossRef](#)]
33. Baltzer, P.; Mann, R.M.; Iima, M.; Sigmund, E.E.; Clauser, P.; Gilbert, F.J.; Martincich, L.; Partridge, S.C.; Patterson, A.; Pinker, K. Diffusion-weighted imaging of the breast—a consensus and mission statement from the EUSOBI International Breast Diffusion-Weighted Imaging working group. *Eur. Radiol.* **2020**, *30*, 1436–1450. [[CrossRef](#)]
34. Iima, M.; Partridge, S.C.; Le Bihan, D. Six DWI questions you always wanted to know but were afraid to ask: Clinical relevance for breast diffusion MRI. *Eur. Radiol.* **2020**, *30*, 2561–2570. [[CrossRef](#)] [[PubMed](#)]
35. Mori, M.; Fujioka, T.; Katsuta, L.; Yashima, Y.; Nomura, K.; Yamaga, E.; Hosoya, T.; Oda, G.; Nakagawa, T.; Kubota, K.; et al. Clinical usefulness of the fast protocol of breast diffusion-weighted imaging using 3T magnetic resonance imaging with a 16-channel breast coil. *Clin. Imaging* **2021**, *78*, 217–222. [[CrossRef](#)]
36. Huang, S.Y.; Seethamraju, R.T.; Patel, P.; Hahn, P.F.; Kirsch, J.E.; Guimaraes, A.R. Body MR imaging: Artifacts, k-Space, and solutions. *Radiographics* **2015**, *35*, 1439–1460. [[CrossRef](#)] [[PubMed](#)]
37. Liney, G.P.; Holloway, L.; Al Harthi, T.; Sidhom, M.; Moses, D.; Juresic, E.; Rai, R.; Manton, D.J. Quantitative evaluation of diffusion-weighted imaging techniques for the purposes of radiotherapy planning in the prostate. *Br. J. Radiol.* **2015**, *88*, 20150034. [[CrossRef](#)]
38. Gatidis, S.; Graf, H.; Weiß, J.; Stemmer, A.; Kiefer, B.; Nikolaou, K.; Notohamprodo, M.; Martirosian, P. Diffusion-weighted echo planar MR imaging of the neck at 3 T using integrated shimming: Comparison of MR sequence techniques for reducing artifacts caused by magnetic-field inhomogeneities. *Magn. Reson. Mater. Phys. Biol. Med.* **2017**, *30*, 57–63. [[CrossRef](#)]
39. Peng, Y.; Li, Z.; Tang, H.; Wang, Y.; Hu, X.; Shen, Y.; Hu, D. Comparison of reduced field-of-view diffusion-weighted imaging (DWI) and conventional DWI techniques in the assessment of rectal carcinoma at 3.0 T: Image quality and histological T staging. *J. Magn. Reson. Imaging* **2018**, *47*, 967–975. [[CrossRef](#)]
40. Baxter, G.C.; Patterson, A.J.; Woitek, R.; Allajbeu, I.; Graves, M.J.; Gilbert, F. Improving the image quality of DWI in breast cancer: Comparison of multi-shot DWI using multiplexed sensitivity encoding to conventional single-shot echo-planar imaging DWI. *Br. J. Radiol.* **2020**, *93*, 20200427. [[CrossRef](#)]
41. Park, J.Y.; Shin, H.J.; Shin, K.C.; Sung, Y.S.; Choi, W.J.; Chae, E.Y.; Cha, J.H.; Kim, H.H. Comparison of readout segmented echo planar imaging (EPI) and EPI with reduced field-of-view diffusion-weighted imaging at 3T in patients with breast cancer. *J. Magn. Reson. Imaging* **2015**, *42*, 1679–1688. [[CrossRef](#)] [[PubMed](#)]
42. Kuhl, C.K.; Schrading, S.; Leutner, C.C.; Morakkabati-Spitz, N.; Wardelmann, E.; Fimmers, R.; Kuhn, W.; Schild, H.H. Mammography, breast ultrasound, and magnetic resonance imaging for surveillance of women at high familial risk for breast cancer. *J. Clin. Oncol.* **2005**, *23*, 8469–8476. [[CrossRef](#)] [[PubMed](#)]
43. Lord, S.; Lei, W.; Craft, P.; Cawson, J.; Morris, I.; Walleiser, S.; Griffiths, A.; Parker, S.; Houssami, N. A systematic review of the effectiveness of magnetic resonance imaging (MRI) as an addition to mammography and ultrasound in screening young women at high risk of breast cancer. *Eur. J. Cancer* **2007**, *43*, 1905–1917. [[CrossRef](#)] [[PubMed](#)]
44. Bonelli, L.A.; Calabrese, M.; Belli, P.; Corcione, S.; Losio, C.; Montemezzi, S.; Pediconi, F.; Petrillo, A.; Zuiani, C.; Camera, L.; et al. MRI versus Mammography plus Ultrasound in Women at Intermediate Breast Cancer Risk: Study Design and Protocol of the MRIB Multicenter, Randomized, Controlled Trial. *Diagnostics* **2021**, *11*, 1635. [[CrossRef](#)]
45. Gelardi, F.; Ragaini, E.M.; Sollini, M.; Bernardi, D.; Chiti, A. Contrast-Enhanced Mammography versus Breast Magnetic Resonance Imaging: A Systematic Review and Meta-Analysis. *Diagnostics* **2022**, *12*, 1890. [[CrossRef](#)]
46. Zhang, H.; Zhang, X.Y.; Wang, Y. Value of magnetic resonance diffusion combined with perfusion imaging techniques for diagnosing potentially malignant breast lesions. *World J. Clin. Cases* **2022**, *10*, 6021–6031. [[CrossRef](#)]
47. Lehman, C.D.; Isaacs, C.; Schnall, M.D.; Pisano, E.D.; Ascher, S.M.; Weatherall, P.T.; Bluemke, D.A.; Bowen, D.J.; Marcom, P.K.; Armstrong, D.K. Cancer yield of mammography, MR, and US in high-risk women: Prospective multi-institution breast cancer screening study. *Radiology* **2007**, *244*, 381–388. [[CrossRef](#)]
48. Woodhams, R.; Matsunaga, K.; Iwabuchi, K.; Kan, S.; Hata, H.; Kuranami, M.; Watanabe, M.; Hayakawa, K. Diffusion-weighted imaging of malignant breast tumors: The usefulness of apparent diffusion coefficient (ADC) value and ADC map for the detection of malignant breast tumors and evaluation of cancer extension. *J. Comput. Assist. Tomogr.* **2005**, *29*, 644–649. [[CrossRef](#)]
49. Yabuuchi, H.; Matsuo, Y.; Okafuji, T.; Kamitani, T.; Soeda, H.; Setoguchi, T.; Sakai, S.; Hatakenaka, M.; Kubo, M.; Sadanaga, N. Enhanced mass on contrast-enhanced breast MR imaging: Lesion characterization using combination of dynamic contrast-enhanced and diffusion-weighted MR images. *J. Magn. Reson. Imaging Off. J. Int. Soc. Magn. Reson. Med.* **2008**, *28*, 1157–1165. [[CrossRef](#)]
50. Kuhl, C.K.; Keulers, A.; Strobel, K.; Schneider, H.; Gaisa, N.; Schrading, S. Not all false positive diagnoses are equal: On the prognostic implications of false-positive diagnoses made in breast MRI versus in mammography/digital tomosynthesis screening. *Breast Cancer Res.* **2018**, *20*, 1–9. [[CrossRef](#)]

51. Zhang, M.; Horvat, J.V.; Bernard-Davila, B.; Marino, M.A.; Leithner, D.; Ochoa-Albiztegui, R.E.; Helbich, T.H.; Morris, E.A.; Thakur, S.; Pinker, K. Multiparametric MRI model with dynamic contrast-enhanced and diffusion-weighted imaging enables breast cancer diagnosis with high accuracy. *J. Magn. Reson. Imaging* **2019**, *49*, 864–874. [[CrossRef](#)] [[PubMed](#)]
52. Egnell, L.; Vidić, I.; Jerome, N.P.; Bofin, A.M.; Bathen, T.F.; Goa, P.E. Stromal collagen content in breast tumors correlates with in vivo diffusion-weighted imaging: A comparison of multi b-Value DWI with histologic specimen from benign and malignant breast lesions. *J. Magn. Reson. Imaging* **2020**, *51*, 1868–1878. [[CrossRef](#)] [[PubMed](#)]
53. Leibfarth, S.; Winter, R.M.; Lyng, H.; Zips, D.; Thorwarth, D. Potentials and challenges of diffusion-weighted magnetic resonance imaging in radiotherapy. *Clin. Transl. Radiat. Oncol.* **2018**, *13*, 29–37. [[CrossRef](#)] [[PubMed](#)]
54. Liu, C.; Wang, K.; Li, X.; Zhang, J.; Ding, J.; Spuhler, K.; Duong, T.; Liang, C.; Huang, C. Breast lesion characterization using whole-lesion histogram analysis with stretched-exponential diffusion model. *J. Magn. Reson. Imaging* **2018**, *47*, 1701–1710. [[CrossRef](#)]
55. Vidić, I.; Egnell, L.; Jerome, N.P.; White, N.S.; Karunamuni, R.; Rakow-Penner, R.; Dale, A.M.; Bathen, T.F.; Goa, P.E. Modeling the diffusion-weighted imaging signal for breast lesions in the $b = 200$ to 3000 s/mm² range: Quality of fit and classification accuracy for different representations. *Magn. Reson. Med.* **2020**, *84*, 1011–1023. [[CrossRef](#)]
56. Bedair, R.; Priest, A.N.; Patterson, A.J.; McLean, M.A.; Graves, M.J.; Manavaki, R.; Gill, A.B.; Abeyakoon, O.; Griffiths, J.R.; Gilbert, F.J. Assessment of early treatment response to neoadjuvant chemotherapy in breast cancer using non-mono-exponential diffusion models: A feasibility study comparing the baseline and mid-treatment MRI examinations. *Eur. Radiol.* **2017**, *27*, 2726–2736. [[CrossRef](#)] [[PubMed](#)]
57. Suo, S.; Cheng, F.; Cao, M.; Kang, J.; Wang, M.; Hua, J.; Hua, X.; Li, L.; Lu, Q.; Liu, J. Multiparametric diffusion-weighted imaging in breast lesions: Association with pathologic diagnosis and prognostic factors. *J. Magn. Reson. Imaging* **2017**, *46*, 740–750. [[CrossRef](#)] [[PubMed](#)]
58. Camps-Herrero, J. Diffusion-weighted imaging of the breast: Current status as an imaging biomarker and future role. *BJR | Open* **2019**, *1*, 20180049. [[CrossRef](#)]
59. Patterson, D.M.; Padhani, A.R.; Collins, D.J. Technology insight: Water diffusion MRI—A potential new biomarker of response to cancer therapy. *Nat. Clin. Pract. Oncol.* **2008**, *5*, 220–233. [[CrossRef](#)]
60. Noij, D.P.; Pouwels, P.J.; Ljumanovic, R.; Knol, D.L.; Doornaert, P.; de Bree, R.; Castelijns, J.A.; de Graaf, P. Predictive value of diffusion-weighted imaging without and with including contrast-enhanced magnetic resonance imaging in image analysis of head and neck squamous cell carcinoma. *Eur. J. Radiol.* **2015**, *84*, 108–116. [[CrossRef](#)]
61. Liu, H.; Zhan, H.; Zhang, Y.; He, G.; Wang, H.; Zhang, Q.; Zheng, L. Comparison of BSGI and MRI as Approaches to Evaluating Residual Tumor Status after Neoadjuvant Chemotherapy in Chinese Women with Breast Cancer. *Diagnostics* **2021**, *11*, 1846. [[CrossRef](#)] [[PubMed](#)]
62. Lee, J.; Kang, B.J.; Park, G.E.; Kim, S.H. The Usefulness of Magnetic Resonance Imaging (MRI) for the Detection of Local Recurrence after Mastectomy with Reconstructive Surgery in Breast Cancer Patients. *Diagnostics* **2022**, *12*, 2203. [[CrossRef](#)] [[PubMed](#)]
63. Turan, U.; Aygun, M.; Duman, B.B.; Kelle, A.P.; Cavus, Y.; Tas, Z.A.; Dirim, A.B.; Irkorucu, O. Efficacy of US, MRI, and F-18 FDG-PET/CT for Detecting Axillary Lymph Node Metastasis after Neoadjuvant Chemotherapy in Breast Cancer Patients. *Diagnostics* **2021**, *11*, 2361. [[CrossRef](#)]
64. Choi, J.H.; Lim, H.I.; Lee, S.K.; Kim, W.W.; Kim, S.M.; Cho, E.; Ko, E.Y.; Han, B.K.; Park, Y.H.; Ahn, J.S. The role of PET CT to evaluate the response to neoadjuvant chemotherapy in advanced breast cancer: Comparison with ultrasonography and magnetic resonance imaging. *J. Surg. Oncol.* **2010**, *102*, 392–397. [[CrossRef](#)] [[PubMed](#)]
65. Chu, W.; Jin, W.; Liu, D.; Wang, J.; Geng, C.; Chen, L.; Huang, X. Diffusion-weighted imaging in identifying breast cancer pathological response to neoadjuvant chemotherapy: A meta-analysis. *Oncotarget* **2018**, *9*, 7088. [[CrossRef](#)]
66. El Ameen, N.F.; Abdel Gawad, E.A.; Abdel Ghany, H.S. Diffusion-weighted imaging versus dynamic contrast-enhanced MRI: A new horizon for characterisation of suspicious breast lesions. *Clin. Radiol.* **2021**, *76*, 80.e81–80.e88. [[CrossRef](#)]
67. van der Hoogt, K.J.J.; Schipper, R.J.; Winter-Warnars, G.A.; Ter Beek, L.C.; Loo, C.E.; Mann, R.M.; Beets-Tan, R.G.H. Factors affecting the value of diffusion-weighted imaging for identifying breast cancer patients with pathological complete response on neoadjuvant systemic therapy: A systematic review. *Insights Into Imaging* **2021**, *12*, 187. [[CrossRef](#)]
68. Lai, H.-W.; Chen, C.-J.; Lin, Y.-J.; Chen, S.-L.; Wu, H.-K.; Wu, Y.-T.; Kuo, S.-J.; Chen, S.-T.; Chen, D.-R. Does Breast Magnetic Resonance Imaging Combined with Conventional Imaging Modalities Decrease the Rates of Surgical Margin Involvement and Reoperation?: A Case–Control Comparative Analysis. *Medicine* **2016**, *95*, e3810. [[CrossRef](#)]
69. Hashem, L.M.B.; Sawy, Y.A.E.; Kamal, R.M.; Ahmed, S.M.; Elmesidy, D.S. The additive role of dynamic contrast-enhanced and diffusion-weighted MR imaging in preoperative staging of breast cancer. *Egypt. J. Radiol. Nucl. Med.* **2021**, *52*, 36. [[CrossRef](#)]
70. Ergul, N.; Kadioglu, H.; Yildiz, S.; Yucel, S.B.; Gucin, Z.; Erdogan, E.B.; Aydin, M.; Muslumanoglu, M. Assessment of multifocality and axillary nodal involvement in early-stage breast cancer patients using 18F-FDG PET/CT compared to contrast-enhanced and diffusion-weighted magnetic resonance imaging and sentinel node biopsy. *Acta Radiol.* **2015**, *56*, 917–923. [[CrossRef](#)]
71. Guo, Y.; Cai, Y.Q.; Cai, Z.L.; Gao, Y.G.; An, N.Y.; Ma, L.; Mahankali, S.; Gao, J.H. Differentiation of clinically benign and malignant breast lesions using diffusion-weighted imaging. *J. Magn. Reson. Imaging Off. J. Int. Soc. Magn. Reson. Med.* **2002**, *16*, 172–178. [[CrossRef](#)] [[PubMed](#)]

72. Chhetri, A.; Li, X.; Rispoli, J.V. Current and emerging magnetic resonance-based techniques for breast cancer. *Front. Med.* **2020**, *7*, 175. [[CrossRef](#)] [[PubMed](#)]
73. Le Bihan, D.; Mangin, J.F.; Poupon, C.; Clark, C.A.; Pappata, S.; Molko, N.; Chabriat, H. Diffusion tensor imaging: Concepts and applications. *J. Magn. Reson. Imaging Off. J. Int. Soc. Magn. Reson. Med.* **2001**, *13*, 534–546. [[CrossRef](#)]
74. Plana, M.N.; Carreira, C.; Muriel, A.; Chiva, M.; Abaira, V.; Emparanza, J.I.; Bonfill, X.; Zamora, J. Magnetic resonance imaging in the preoperative assessment of patients with primary breast cancer: Systematic review of diagnostic accuracy and meta-analysis. *Eur. Radiol.* **2012**, *22*, 26–38. [[CrossRef](#)] [[PubMed](#)]
75. Scaranelo, A.M.; Degani, H.; Grobgeld, D.; Talbot, N.; Bodolai, K.; Furman-Haran, E. Effect of IV Administration of a Gadolinium-Based Contrast Agent on Breast Diffusion-Tensor Imaging. *Am. J. Roentgenol.* **2020**, *215*, 1030–1036. [[CrossRef](#)] [[PubMed](#)]
76. Nissan, N.; Allweis, T.; Menes, T.; Brodsky, A.; Paluch-Shimon, S.; Haas, I.; Golan, O.; Miller, Y.; Barlev, H.; Carmon, E. Breast MRI during lactation: Effects on tumor conspicuity using dynamic contrast-enhanced (DCE) in comparison with diffusion tensor imaging (DTI) parametric maps. *Eur. Radiol.* **2020**, *30*, 767–777. [[CrossRef](#)]
77. Abdelhady, D.; Abdelbary, A.; Afifi, A.H.; Abdelhamid, A.E.; Hassan, H.H.M. Diffusion tensor imaging on 3-T MRI breast: Diagnostic performance in comparison to diffusion-weighted imaging. *Egypt. J. Radiol. Nucl. Med.* **2021**, *52*, 98. [[CrossRef](#)]
78. Onaygil, C.; Kaya, H.; Ugurlu, M.U.; Aribal, E. Diagnostic performance of diffusion tensor imaging parameters in breast cancer and correlation with the prognostic factors. *J. Magn. Reson. Imaging: JMIR* **2017**, *45*, 660–672. [[CrossRef](#)]
79. Furman-Haran, E.; Nissan, N.; Ricart-Selma, V.; Martinez-Rubio, C.; Degani, H.; Camps-Herrero, J. Quantitative evaluation of breast cancer response to neoadjuvant chemotherapy by diffusion tensor imaging: Initial results. *J. Magn. Reson. Imaging* **2018**, *47*, 1080–1090. [[CrossRef](#)]
80. Mao, C.; Jiang, W.; Huang, J.; Wang, M.; Yan, X.; Yang, Z.; Wang, D.; Zhang, X.; Shen, J. Quantitative Parameters of Diffusion Spectrum Imaging: HER2 Status Prediction in Patients with Breast Cancer. *Front. Oncol.* **2022**, *12*, 817070. [[CrossRef](#)]
81. Cho, E.; Baek, H.J.; Szczepankiewicz, F.; An, H.J.; Jung, E.J.; Lee, H.J.; Lee, J.; Gho, S.M. Clinical experience of tensor-valued diffusion encoding for microstructure imaging by diffusional variance decomposition in patients with breast cancer. *Quant. Imaging Med. Surg.* **2022**, *12*, 2002–2017. [[CrossRef](#)] [[PubMed](#)]
82. Wilmes, L.J.; Li, W.; Shin, H.J.; Newitt, D.C.; Proctor, E.; Harnish, R.; Hylton, N.M. Diffusion tensor imaging for assessment of response to neoadjuvant chemotherapy in patients with breast cancer. *Tomography* **2016**, *2*, 438. [[CrossRef](#)] [[PubMed](#)]
83. Menning, S.; de Ruijter, M.B.; Veltman, D.J.; Boogerd, W.; Oldenburg, H.S.; Reneman, L.; Schagen, S.B. Changes in brain white matter integrity after systemic treatment for breast cancer: A prospective longitudinal study. *Brain Imaging Behav.* **2018**, *12*, 324–334. [[CrossRef](#)] [[PubMed](#)]
84. Zhou, J.; Payen, J.-F.; Wilson, D.A.; Traystman, R.J.; van Zijl, P. Using the amide proton signals of intracellular proteins and peptides to detect pH effects in MRI. *Nat. Med.* **2003**, *9*, 1085–1090. [[CrossRef](#)]
85. Zaric, O.; Farr, A.; Rodriguez, E.P.; Mlynarik, V.; Bogner, W.; Gruber, S.; Asseryanis, E.; Singer, C.F.; Trattnig, S. 7T CEST MRI: A potential imaging tool for the assessment of tumor grade and cell proliferation in breast cancer. *Magn. Reson. Imaging* **2019**, *59*, 77–87. [[CrossRef](#)]
86. Crescenzi, R.; Donahue, P.M.; Mahany, H.; Lants, S.K.; Donahue, M.J. CEST MRI quantification procedures for breast cancer treatment-related lymphedema therapy evaluation. *Magn. Reson. Med.* **2020**, *83*, 1760–1773. [[CrossRef](#)]
87. Someya, Y.; Iima, M.; Imai, H.; Yoshizawa, A.; Kataoka, M.; Isoda, H.; Le Bihan, D.; Nakamoto, Y. Investigation of breast cancer microstructure and microvasculature from time-dependent DWI and CEST in correlation with histological biomarkers. *Sci. Rep.* **2022**, *12*, 6523. [[CrossRef](#)]
88. Meng, N.; Wang, X.; Sun, J.; Han, D.; Bai, Y.; Wei, W.; Wang, Z.; Jia, F.; Wang, K.; Wang, M. A comparative study of the value of amide proton transfer-weighted imaging and diffusion kurtosis imaging in the diagnosis and evaluation of breast cancer. *Eur. Radiol.* **2021**, *31*, 1707–1717. [[CrossRef](#)]
89. Jensen, J.H.; Helpert, J.A.; Ramani, A.; Lu, H.; Kaczynski, K. Diffusional kurtosis imaging: The quantification of non-gaussian water diffusion by means of magnetic resonance imaging. *Magn. Reson. Med. Off. J. Int. Soc. Magn. Reson. Med.* **2005**, *53*, 1432–1440. [[CrossRef](#)]
90. Jensen, J.H.; Helpert, J.A. MRI quantification of non-Gaussian water diffusion by kurtosis analysis. *NMR Biomed.* **2010**, *23*, 698–710. [[CrossRef](#)]
91. Wang, W.; Zhang, X.; Zhu, L.; Chen, Y.; Dou, W.; Zhao, F.; Zhou, Z.; Sun, Z. Prediction of Prognostic Factors and Genotypes in Patients with Breast Cancer Using Multiple Mathematical Models of MR Diffusion Imaging. *Front. Oncol.* **2022**, *12*, 825264. [[CrossRef](#)] [[PubMed](#)]
92. Fardanesh, R.; Marino, M.A.; Avendano, D.; Leithner, D.; Pinker, K.; Thakur, S.B. Proton MR spectroscopy in the breast: Technical innovations and clinical applications. *J. Magn. Reson. Imaging* **2019**, *50*, 1033–1046. [[CrossRef](#)] [[PubMed](#)]
93. Baltzer, P.A.; Dietzel, M. Breast lesions: Diagnosis by using proton MR spectroscopy at 1.5 and 3.0 T—systematic review and meta-analysis. *Radiology* **2013**, *267*, 735–746. [[CrossRef](#)] [[PubMed](#)]
94. Sharma, U.; Jagannathan, N.R. In vivo MR spectroscopy for breast cancer diagnosis. *BJR Open* **2019**, *1*, 20180040. [[CrossRef](#)]
95. Galati, F.; Luciani, M.L.; Caramanico, C.; Moffa, G.; Catalano, C.; Pediconi, F. Breast magnetic resonance spectroscopy at 3 T in biopsy-proven breast cancers: Does Choline peak correlate with prognostic factors? *Investig. Radiol.* **2019**, *54*, 767–773. [[CrossRef](#)]

96. Thakur, S.B.; Horvat, J.V.; Hancu, I.; Sutton, O.M.; Bernard-Davila, B.; Weber, M.; Oh, J.H.; Marino, M.A.; Avendano, D.; Leithner, D. Quantitative in vivo proton MR spectroscopic assessment of lipid metabolism: Value for breast cancer diagnosis and prognosis. *J. Magn. Reson. Imaging* **2019**, *50*, 239–249. [[CrossRef](#)]
97. Prvulovic Bunovic, N.; Sveljo, O.; Kozic, D.; Boban, J. Is Elevated Choline on Magnetic Resonance Spectroscopy a Reliable Marker of Breast Lesion Malignancy? *Front. Oncol.* **2021**, *11*, 610354. [[CrossRef](#)]
98. Chen, L.; Liu, M.; Bao, J.; Xia, Y.; Zhang, J.; Zhang, L.; Huang, X.; Wang, J. The correlation between apparent diffusion coefficient and tumor cellularity in patients: A meta-analysis. *PLoS ONE* **2013**, *8*, e79008. [[CrossRef](#)]